07

Impedance spectroscopy study of tandem solar cells based on c-Si with a top layer perovskite nanocrystals $CsPbBr_3$ and $CsPbI_3$

© L. Boudjemila,[1,2] G.V. Nenashev,[2] V.G. Malyshkin,[2] E.I. Terukov,[2] A.N. Aleshin[2]

[1]Peter the Great Saint-Petersburg Polytechnic University,
195251 St. Petersburg, Russia
[2]Ioffe Institute,
194021 St. Petersburg, Russia
e-mail: aleshin@transport.ioffe.ru

Received February 19, 2024
Revised February 19, 2024
Accepted February 22, 2024

The deposition of an additional layer of nanoparticles is a widely used method for improving optical and electrical characteristics of semiconductor solar cells (SCs). We present the results of studies of impedance spectroscopy (IS) in operating sandwich structures based on films of nanocrystals (NCs) of inorganic perovskites of lead halides $CsPbI_3$ and $CsPbBr_3$ deposited on the surface of a SCs based on crystalline silicon (c-Si). The IS results show that under identical conditions the Cole-Cole plots for both structures are in a good agreement with the equivalent circuit model and represents series resistance, recombination resistance and geometric capacitance, respectively, which arise due to charge accumulation, charge transfer resistance and/or additional interfacial electronic states. It was found that adding of the $CsPbI_3$ layer enhances the photo response under bias, but such a photo response leads to a decrease in conductivity. On the contrary, adding of the $CsPbBr_3$ layer blocks the photo response under bias but slightly improves the photo response for the zero bias. The obtained results provide the way to improve the performance of next generation of tandem c-Si SCs with perovskite NCs upper layers.

Keywords: Impedance spectroscopy, Solar cell, Perovskites, Nanocrystals, Crystalline silicon.

DOI: 10.61011/JTF.2024.04.57535.43-24

Introduction

Recently, extensive studies have been carried out for the sake of improvement of the efficiency of tandem c-Si solar cells (SCs) based on heterostructures by applying films of metalorganic perovskites. Modification of the surface of c-Si SCs with films of metalorganic perovskites is considered to be one of the most promising areas [1] thanks to a high absorption coefficient in these materials within the visible spectrum [2], the ability to form multilayer heterostructures based on them [3], quite high mobility of the charge carriers [4], as well as relatively low cost of production thereof. On the other hand, optical resonance nanostructures, such as nanocrystals (NCs) of inorganic perovskites, could improve the properties of c-Si SCs as well [5].

Impedance spectroscopy (IS) is a universal method for characterization of SCs to assess their electric properties and to determine electrochemical processes, as well as to make a profile of electronic structure in solid-state devices [6–8]. Optoelectronic studies of these structures were performed in the previous paper [5]. Morphological studies carried out by using the atomic-force microscopy (AFM) revealed white spherical dots of various density, shape and size [5]. Here in the authors present the results of IS for the structures c-Si/$CsPbBr_3$ (NCs) and c-Si/$CsPbI_3$ (NCs) and discuss their current-voltage characteristics. The IS results demonstrate that under identical conditions the measured Nyquist plots have a good correlation with the simulated ones. Equivalent circuit model is proposed, which takes into account the ohmic resistance, recombination resistance and the geometric capacitance, which occur due to charge accumulation, resistance to the charge transfer and/or additional interphase electronic states. We found that addition of a $CsPbI_3$ NC layer improves photoresponse in the bias conditions, however, such an improvement results in reduction of conductivity for direct current. Vice versa, inclusion of a $CsPbBr_3$ NC layer blocks the photoresponse under bias, but intensifies the photoresponse insignificantly at the absence of applied voltage.

1. Experiment details

1.1. Preparation of samples

Herein we used SCs made of single crystal silicon c-Si, provided by the Research Center for Thin-Film Technologies in Power Engineering of the Ioffe Physical-Technical Institute. The structure of a standardized SC shown in Fig. 1, *a* includes a silicon crystalline substrate of n-type (c-Si) oriented (100), both sides of which are coated with a layer of amorphous hydrogenated silicon carbide as a solid solution Si_xC_{x-1}:H (where $0.8 < x < 0.90$) with the thickness of $0.5-2$ nm; non-alloyed layer of amorphous hydrogenated silicon with the thickness of $2-5$ nm, whose front face (the emission side) is coated with p-doped layer

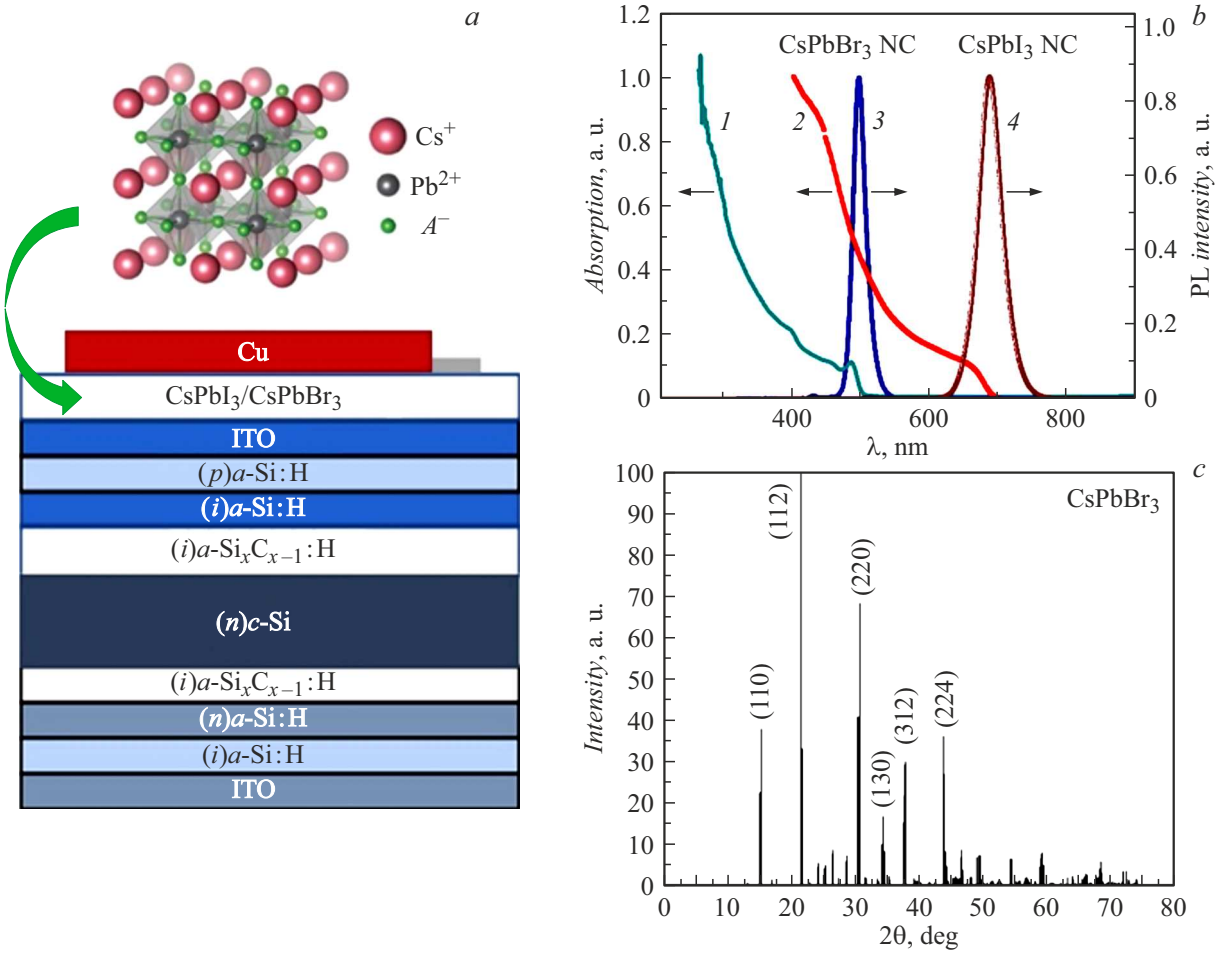

Figure 1. *a* — structure of CS and NC $Cs^{+}Pb^{2+}A_3^{-}$ perovskites, where *A* — I, Br; *b* — spectra of absorption of pure films of NC $CsPbBr_3$ (line *1*), and $CsPbI_3$ (line *2*) on quartz substrates; the same plot shows PL spectra of pure NCs $CsPbBr_3$ (line *3*) and $CsPbI_3$ (line *4*), curves *1* and *3*, as well as *2* and *4* are presented in the papers [11,12] accordingly; *c* — the results of XRD — studies of the film of NCs $CsPbBr_3$.

of amorphous hydrogenated silicon with the thickness of 5−20 nm; the layer of indium-tin oxide (ITO) with the thickness of 90−110 nm. The rear side of crystalline substrate is serially coated by alloyed *n*-layer of amorphous hydrogenated silicon with the thickness of 10−20 nm, and a layer of ITO with the thickness of 40−80 nm [9,10].

Toluene solutions containing NCs of $CsPbI_3$ or NCs of $CsPbBr_3$ were synthesized by hot injection, the same as in our previous studies [11,12] and in accordance with [13,14]. In the hot injection method, precursor compounds are dissolved in a solvent with high boiling point and heated up to the temperature exceeding the solvent's boiling point. The same growth temperature was used for both NCs. Then, the mixture was added by a solvent with lower boiling point for faster cooling down and creation of quantum dots material nucleating centers, which leads to creation of fine homogeneous particles. The reaction mixture is kept at a lower temperature for some time to grow up quantum dots, after which a sealing agent is added for stabilization of particles. Thereafter, quantum dots have been flushed with a solvent in order to remove excess ligands and by-products, and could be dispersed again in a desired solvent for further application. Finally, these solutions of NCs were applied onto substrates made of *c*-Si by centrifugation with the use of Chemat Technology spin-coater KW-4A centrifuge at 2000 rpm during 30 s. The film thickness for the sample $CsPbI_3$ and the sample $CsPbBr_3$ was 30−40 nm and 100−150 nm respectively [5]. To study optical characteristics earlier we had measured the absorption and photoluminescence (PL). Fig. 1, *b* represents the spectra of absorption and PL of pure films $CsPbI_3$ NCs [11] and $CsPbBr_3$ NCs [12] on quartz substrates. Fig. 1, *c* presents the results of XRD-study of the film of NCs $CsPbBr_3$.

1.2. IS measurements

IS measurements were carried out in the darkness and when illuminated by sunlight imitator with the use of Elins impedance meter Z-500PX by the method described in our

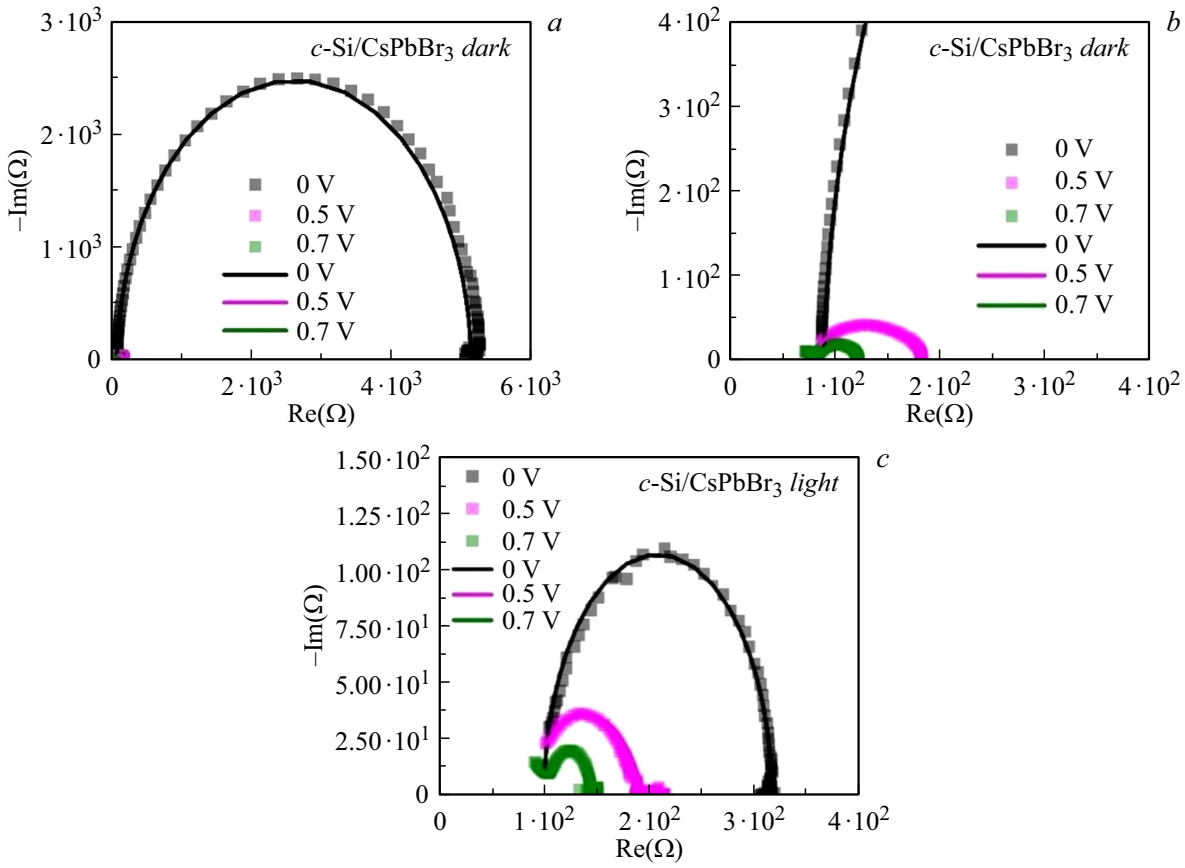

Figure 2. Impedance diagram for *a* — *c*-Si/$CsPbBr_3$ in the darkness; *b* — lower scale within the high-frequency region (*c*-Si/$CsPbBr_3$ in the darkness); *c* — *c*-Si/$CsPbBr_3$ when illuminated and at different bias voltages. Dots — real impedance, lines — impedance imitation.

previous paper [15]. The top electrode was made of copper. The measurements were carried out under direct bias within the range from 0 to 1 V within the frequency range from 10 Hz to 0.5 MHz. The IS data were analyzed by using a licensed software Z-View. In order to suppress external interferences, the samples under study were placed inside a copper box.

2. Results and discussion

For better understanding of the specifics of the transfer mechanism in our samples, we studied IS in similar conditions (in darkness and under illumination for conciseness) for the samples *c*-Si of SCs with top layers of NCs $CsPbBr_3$ and $CsPbI_3$, as well as for pure sample *c*-Si SCs (without applying the top layer of NCs). Fig. 2, *a,b* shows plots of impedance response for the sample *c*-Si/$CsPbBr_3$ in the darkness (Fig. 2, *a*) and when illuminated (Fig. 2, *b*). In the same way, Fig. 3 shows plots of impedance response for the sample *c*-Si/$CsPbI_3$ in the darkness (Fig. 3, *a*) and when illuminated (Fig. 3, *b*), and Fig. 4, *a, b* — plots of impedance response for pure sample *c*-Si in the darkness (Fig. 4, *a*) and when illuminated (Fig. 4, *b*). These plots represent the data of impedance response, where Im (Ω) — is an imaginary part of complex resistance, and Re (Ω) — is a real part of the complex resistance. Semicircle at a higher frequency is associated with the charge transfer and recombination through the structure/contacts, and semicircle at a lower frequency — is associated with the recombination of charge carriers, relaxation of dielectric and migration of ions within the structure layers [16]. Parasite inductive tail on the impedance response plot at high frequencies are attributed to parasite inductivity originating from cables and electrodes [17].

The plots of impedance response with different bias voltages were simulated by means of equivalent circuits shown in Fig. 5 (for two cases: at the voltage of 0.5 V and lower and at the voltage of 0.7 V and higher). In Fig. 5, *a* equivalent scheme consists of a resistor R_1 included in series with parallel combination of the constant element of the phase CPE_1 and the resistance R_2. This equivalent scheme provides a perfect alignment of data for a series of applied bias voltages [18]. The element R_1 represents resistive losses at electrodes and corresponds to the bias from zero to semicircle and Re axis crossing at high frequencies. The element R_2 corresponds to the semicircle diameter and decreases in response to the sample bias increase. It can be explained by the decrease of volume resistance as a result of introduction of the charge carriers [19,20]. CPE is an non-ideal capacitor and associated with $p^+ - n$-

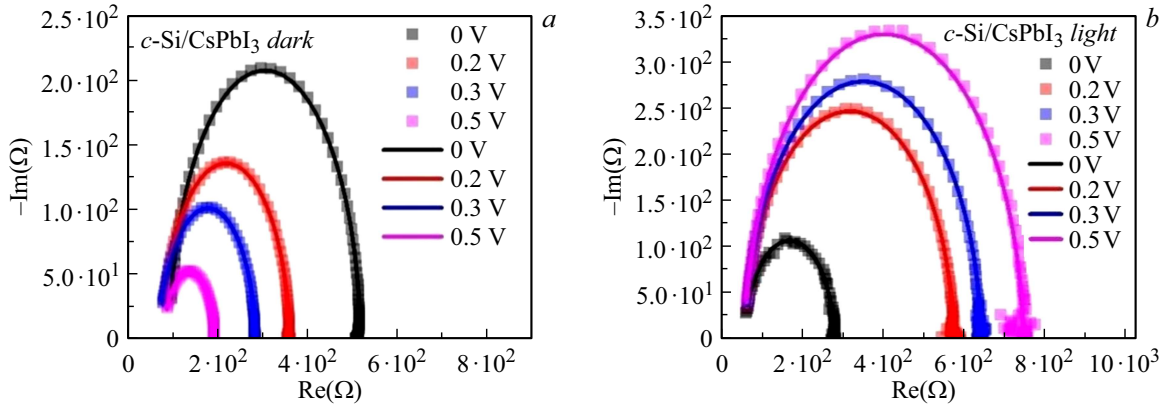

Figure 3. Impedance diagram for *a* — *c*-Si/$CsPbI_3$ in the darkness and *b* — *c*-Si/$CsPbI_3$ when illuminated and at different bias voltages. Dots — real impedance; lines — impedance imitation.

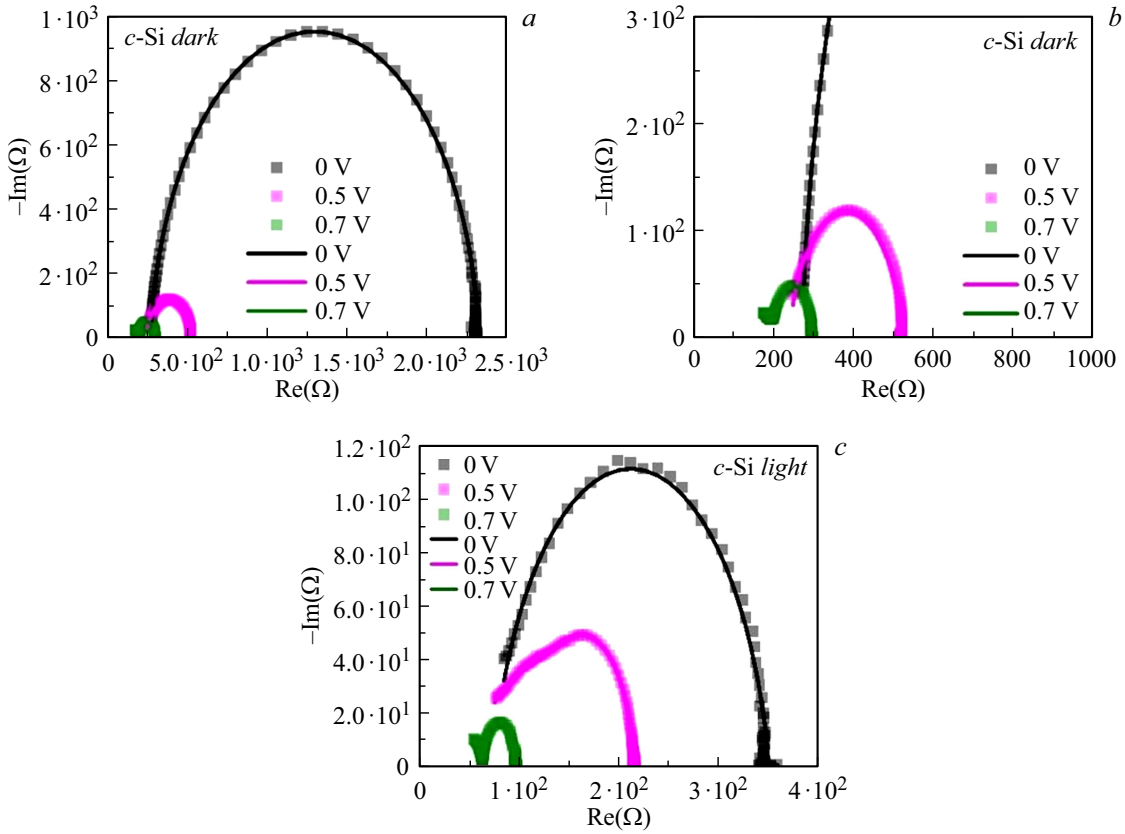

Figure 4. Impedance diagram for *a* — *c*-Si in the darkness; *b* — lower scale within a high-frequency region (*c*-Si in the darkness); *c* — *c*-Si when illuminated and at different bias voltages. Dots — real impedance; lines — impedance imitation.

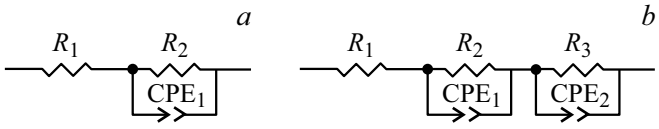

Figure 5. Model of equivalent circuits for *a* — at the voltage of 0.5 V and lower; *b* — at the voltage of 0.7 V and higher.

transition in the layer Si [18] and non-uniform distribution of the dielectric relaxation time, which is manifested due to heterogeneities in the perovskite layer [21]. Significant decrease of the semicircle arc diameter is observed with the increase of the bias voltage. However, for the sample *c*-Si/$CsPbI_3$ the arc diameter is increased, which is explained by the effect of negative photoresponse [22–24]. Fig. 5, *b* additionally contains the constant element of the phase CPE_2 and the resistance R_3, which describe the tail on the plots of impedance response within the high-frequency

Numerical values of parameters for every model

Top layer	R_1	R_2	T_1	P_1	R_3	T_2	P_2
$CsPbBr_3$_0_dark	89.6	5065	$1.32 \cdot 10^{-8}$	0.98691			
$CsPbBr_3$_light	100	218	$1.61 \cdot 10^{-8}$	0.9907			
$CsPbBr_3$_05_dark	76.9	106.5	$1.26 \cdot 10^{-7}$	0.84964			
$CsPbBr_3$_05_light	84.1	111.1	$5.13 \cdot 10^{-7}$	0.73349			
$CsPbBr_3$_07_dark	46.9	38.36	$5.48 \cdot 10^{-7}$	0.69104	37.11	$8.44 \cdot 10^{-}7$	0.99971
$CsPbBr_3$_07_light		111.2	$1.57 \cdot 10^{-6}$	0.49134	35.64	$6.43 \cdot 10^{-7}$	0.99792
$CsPbI_3$_0_dark	92.83	424.2	$1.30 \cdot 10^{-8}$	0.98431			
$CsPbI_3$_0_light	57.35	219.8	$1.62 \cdot 10^{-8}$	0.97827			
$CsPbI_3$_02_dark	77.69	281.3	$1.59 \cdot 10^{-8}$	0.97545			
$CsPbI_3$_02_light	58.44	513.6	$1.37 \cdot 10^{-8}$	0.97318			
$CsPbI_3$_03_dark	73.02	210	$1.73 \cdot 10^{-8}$	0.97325			
$CsPbI_3$_03_light	58.55	581.2	$1.30 \cdot 10^{-8}$	0.97284			
$CsPbI_3$_05_dark	80.3	111.6	$2.37 \cdot 10^{-8}$	0.95978			
CsPbI3_05_light	58.66	684.8	$1.15 \cdot 10^{-8}$	0.97567			
$CsPbI_3$_07_dark	60.89	32.4	$3.53 \cdot 10^{-7}$	1	43.74	$1.08 \cdot 10^{-6}$	0.7
c-Si pure_0_dark	270	2044	$1.27 \cdot 10^{-8}$	0.95275			
c-Si pure_0_light	73.66	276.8	$6.92 \cdot 10^{-8}$	0.86319			
c-Si pure_05_dark	239.1	281.7	$5.54 \cdot 10^{-8}$	0.8839			
c-Si pure_05_light	52.7	62.01	$1.12 \cdot 10^{-7}$	1	101	$9.90 \cdot 10^{-7}$	0.6774
c-Si pure_07_dark	103.2	103.5	$8.56 \cdot 10^{-7}$	0.58	88.79	$2.45 \cdot 10^{-7}$	1
c-Si pure_07_light	36.93	26.62	$3.61 \cdot 10^{-8}$	0.90097	33.35	$2.87 \cdot 10^{-6}$	0.99822

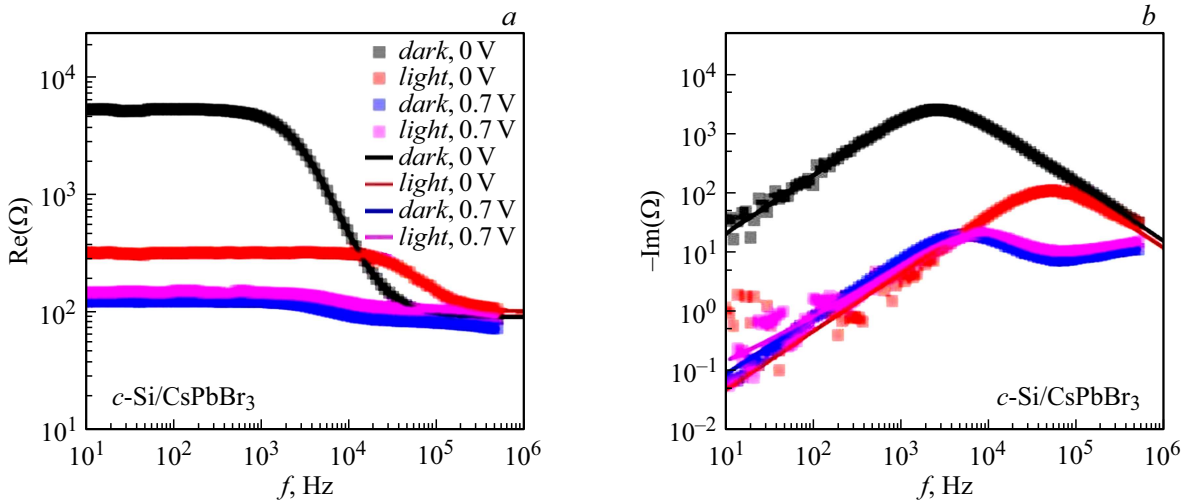

Figure 6. Frequency dependences of real (a) and imaginary (b) parts of the complex resistance for c-Si/$CsPbBr_3$ sample in the darkness and when illuminated at different bias voltages. Dots — real impedance, lines — impedance imitation.

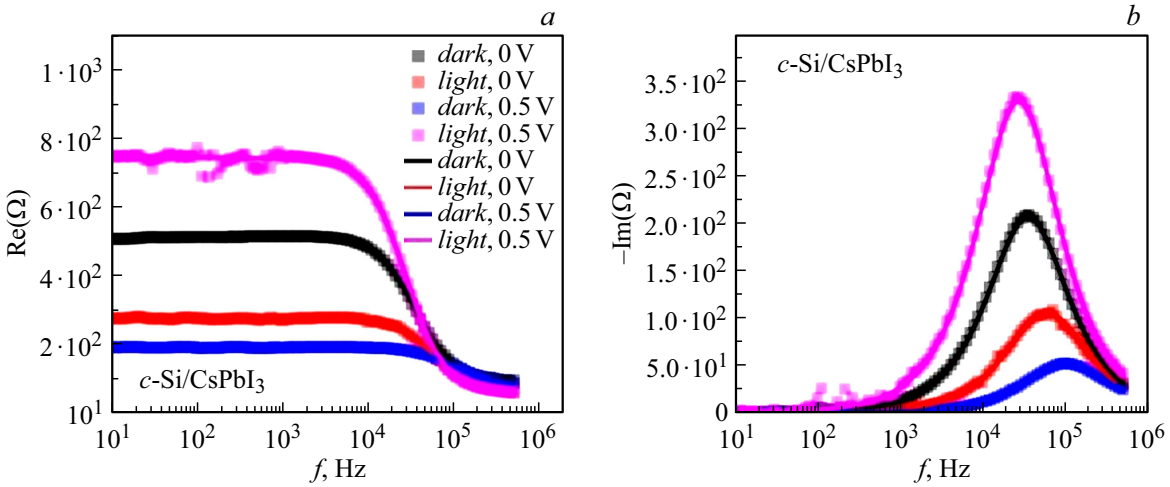

Figure 7. Frequency dependences of real (a) and imaginary (b) parts of the complex resistance for c-Si/$CsPbI_3$ sample in the darkness and when illuminated at different bias voltages. Dots — real impedance, lines — impedance imitation.

region at high bias voltages. The presence of such standard semicircles on the plots of impedance response means that the SCs under study have an ideal electric response, do not demonstrate explicit degradation and are characterized in a good stability [25].

Compared to a pure sample c-Si, the sample c-Si/$CsPbBr_3$ demonstrates far more significant change of the impedance response in the darkness under the applied bias voltage due to higher semicircle at zero bias voltage and lower semicircle at other bias voltages. Any significant changes in the impedance characteristic when illuminated by a sunlight imitator were not found for that sample.

The sample c-Si/$CsPbI_3$ against the sample c-Si demonstrates less significant change in the impedance characteristic in the darkness, but far better conductivity. The light impact on the sample c-Si/$CsPbI_3$ leads to the effect of negative photoconductivity [22–24].

The analysis of alignment parameters of the chain elements for all samples without applying the bias voltage was carried out by means of ZView software. Each plot of the impedance response is described by four parameters: R_1, R_2, T and P (for the capacitance $C = T$, $P = 1$). The numerical values of these parameters are given in Table. The errors of all resulting parameters are less than 5%.

The impedance response in different conditions (in the darkness and when illuminated at different bias voltages) for all samples was compared with the frequency dependences of real (a) and imaginary (b) parts in Fig. 6 (for the sample c-Si/$CsPbBr_3$), in Fig. 7 (for the sample c-Si/$CsPbI_3$) and in Fig. 8 (for the sample c-Si). For the sample c-Si/$CsPbBr_3$ one can note the impact of light on the conductivity at zero bias voltage, which leads to decrease of resistance and a significant bias of the resistance peak towards high-frequency region (capacitance decrease). The photoconductivity effect becomes insignificant when the bias is applied. Moreover, the bias is characterized in appearance of the second peak within the high-frequency region in Fig. 6, b. It can be explained by the appearance of parasite inductivity, which becomes noticeable at high values of bias voltage [16]. For the sample c-Si/$CsPbI_3$ the light impact on conductivity is noticeable at any bias voltages. But high bias values lead to the effect of negative photoconductivity [19–21]. Compared to the sample c-Si/$CsPbBr_3$ the peaks of imaginary part of the complex resistance for the sample c-Si/$CsPbI_3$ are sharper and demonstrate lower biases on the frequency axis.

For the sample c-Si the light impact on the conductivity is noticeable at any bias voltages versus the sample c-Si/$CsPbBr_3$, and the effect of negative photoconductivity is not observed versus the sample c-Si/$CsPbI_3$.

Therefore, we may conclude that SCs with applied films of NCs of inorganic perovskite demonstrate the properties, which are nearly similar to those of pure c-Si SC, however, certain differences were noted.

The resistance of recombination of the sample c-Si/$CsPbBr_3$ and pure sample c-Si changes in a similar way, depending on the applied bias voltage. Both recombination resistance and serial resistance decrease as far as the applied bias voltage increases. On the other hand, the sample c-Si/$CsPbI_3$ demonstrates totally different behavior. The recombination resistance and the serial resistance of the sample c-Si/CsPI3 increase as far as the applied voltage increases. Non-ideal capacitor demonstrates the dynamics of the charge carriers in the tandem of a-Si:H/a-Si_xC_x:H/c-Si SCs. It should be noted that the film of NCs $CsPbI_3$ intensifies the photoresponse with the increase of the bias voltage, however, such a photoresponse leads to decrease in the direct current. Vice versa, the film of NCs $CsPbBr_3$ blocks photoresponse with the applied bias voltage, but a bit improves the photoresponse at zero bias voltage. When the applied voltage exceeds 0.6 V, new semicircles are formed. This effect was explained by the second equivalent circuits

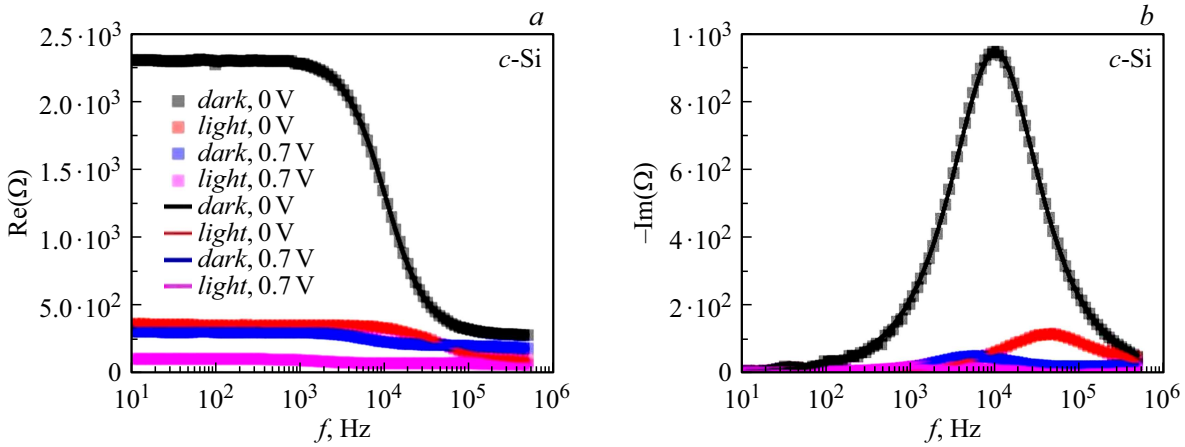

Figure 8. Frequency dependences of real (*a*) and imaginary (*b*) parts of complex resistance for *c*-Si sample in the darkness and when illuminated at different bias voltages. Dots — real impedance, lines — impedance imitation.

Conclusion

The study presents the results of IS studies in multilayered structures based on the films of NCs of inorganic perovskites $CsPbI_3$ and $CsPbBr_3$ applied onto the surface of SCs based on *c*-Si. The IS results show that under identical conditions, the impedance response plots for both structures have a good correlation with the models of equivalent circuits. These models of equivalent circuits are represented by the elements of resistance and phase constant (which describes the effects that occur due to charge accumulation, resistance to the charge transfer and/or additional interphase electronic states). The numerical values of the parameters R, T, and P were obtained for every model of the equivalent circuits (the errors of all resulting parameters are less than 5%). It was found that the addition of a layer of NCs $CsPbI_3$ intensifies the photoresponse with the increase of the bias voltage, however, such a photoresponse leads to a decrease in the conductivity (effect of negative photoconductivity). Vice versa, the addition of a layer of NCs $CsPbBr_3$ blocks photoresponse with the increase of the bias voltage, but a bit improves the photoresponse at zero bias voltage.

This study provides a view of the processes in tandem SCs based on *c*-Si with top layers of NCs of inorganic perovskites $CsPbBr_3$ ($CsPbI_3$) by analysis of impedance spectra in different conditions. The results obtained make it possible to improve the performance characteristics of the next generation of tandem *c*-Si SCs with top layers of inorganic perovskite NCs.

Acknowledgments

The authors thank I.P. Shcherbakov for their help in studying photoluminescence.

Conflict of interest

The authors declare that they have no conflict of interest.

References

[1] G. Eperon, M. Hörantner, H. Snaith. Nat. Rev. Chem., **1**, 0095 (2017). DOI: 10.1038/s41570-017-0095
[2] C. Gao, D. Du, W. Shen. Carb Neutrality, **1**, 9 (2022). DOI: 10.1007/s43979-022-00003-x
[3] A. Al-Ashouri, A. Magomedov, M. Roß, M. Jošt, M. Talaikis, G. Chistiakova, R. Schlatmann. Science, **366** (6468), 857 (2019). DOI: 10.1126/science.abd4016
[4] F. Sahli, J. Werner, B.A. Kamino, M. Bräuninger, R. Monnard, B. Paviet-Salomon. Nature Mater., **17** (9), 820 (2018). DOI: 10.1038/s41563-018-0115-4
[5] L. Boudjemila, A.N. Aleshin, V.G. Malyshkin, P.A. Aleshin, I.P. Shcherbakov, V.N. Petrov, E.I. Terukov. Physics Solid State, **64**, 1670 (2022). DOI:10.21883/PSS.2022.11.54189.418
[6] E. Hauff, D. Klotz. J. Mater. Chem. C, **10**, 742 (2022). DOI: 10.1039/D1TC04727B
[7] M.M. Shehata, T.N. Truong, R. Basnet, H.T. Nguyen, D.H. Macdonald, L.E. Black. Solar Energy Materials Solar Cells, **251**, 112167 (2023). DOI: 10.1016/j.solmat.2022.112167
[8] B. Hailegnaw, N.S. Sariciftci, M.C. Scharber. Phys. Status Solidi A, **22**, 2000291 (2020). DOI: 10.1002/pssa.202000291
[9] E. Terukov, A. Kosarev, A. Abramov, E. Malchukova. Solar Panels and Photovoltaic Materials, **5** (2018). DOI: 10.5772/intechopen.75013
[10] M. Masuko, M. Shigematsu, T. Hasiguchi, D. Fujishima, M. Kai, N. Yoshimira, T. Yamaguchi, Y. Ichihashi, T. Mishima, N. Matsubara, T. Yamanishi, T. Takahama, M. Taguchi, E. Maruyama, S. Okamoto. IEEE J. Photovoltaics, **4**, 1433 (2014). DOI: 10.1109/JPHOTOV.2014.2352151
[11] A.N. Aleshin, I.P. Shcherbakov, E.V. Gushchina, L.B. Matyushkin, V.A. Moshnikov. Organic Electron., **50**, 213 (2017). DOI: 10.1016/j.orgel.2017.08.004
[12] A.N. Aleshin, I.P. Shcherbakov, O.P. Chikalova-Luzina, L.B. Matyushkin, M.K. Ovezov, A.M. Ershova, I.N. Trapeznikova, V.N. Petrov. Synthetic Metals, **260**, 116291 (2020). DOI: 10.1016/j.synthmet.2020.116291
[13] L. Protesescu, S. Yakunin, M.I. Bodnarchuk, F. Krieg, R. Caputo, C.H. Hendon, M.V. Kovalenko. Nano Lett., **15**, 3692 (2015). DOI: 10.1021/nl5048779

[14] A.K. Soni, R. Joshi, R.S. Ningthoujam. *Hot Injection Method for Nanoparticle Synthesis: Basic Concepts, Examples and Applications*. In: A.K. Tyagi, R.S. Ningthoujam (eds). *Handbook on Synthesis Strategies for Advanced Materials* (Indian Institute of Metals Series. Springer, Singapore, 2021), DOI: 10.1007/978-981-16-1807-9_13
[15] A.M. Ivanov, G.V. Nenashev, A.N. Aleshin. J. Mater. Sci.: Mater. Electron., **33**, 21666 (2022). DOI: 10.1007/s10854-022-08955-7
[16] H. Zhang, X. Qiao, Y. Shen, T. Moehl, S.M. Zakeeruddin, M. Gratzel, M. Wang. J. Mater. Chem. A, **3**, 11762 (2015). DOI: 10.1039/C5TA02206A
[17] J. Panigrahi, R. Singh, N. Batra, J. Gope, M. Sharma, P. Pathi, S. Srivastava, C. Rauthan, P. Singh. Sol. Energy, **136**, 412 (2016). DOI: 10.1016/j.solener.2016.06.041
[18] Y. Yorozu, M. Hirano, K. Oka, Y. Tagawa. IEEE Transl. J. Magn. Jpn., **2**, 740 (1987).
[19] J. Li, R. Gao, F. Gao, J. Lei, H. Wang, X. Wu, J. Li, H. Liu, X. Hua, S. Liu. J. Alloys Comp., **818**, 152903 (2020). DOI: 10.1016/j.jallcom.2019.152903
[20] G. Tong, T. Chen, H. Li, W. Song, Y. Chang, J. Liu, L. Yu, J. Xu, Y. Qi, Y. Jiang. Solar RRL, **3**, 1900030 (2019). DOI: 10.1002/solr.201900030
[21] V. Srivastava, A. Alexander, B. Anitha, M.A.G. Namboothiry. Sol. Energy Mat. Sol. Cells, **237**, 111548 (2022). DOI: 10.1016/j.solmat.2021.111548
[22] N.K. Tailor, C.A. Aranda, M. Saliba, S. Satapathi. ACS Mater. Lett., **4**, 2298 (2022). DOI: 10.1021/acsmaterialslett.1c00242
[23] H. Jin, Y. Chen, L. Zhang, R. Wan, Z. Zou, H. Li, Y. Gao. Nanotechnology, **32**, 085202 (2020). DOI: 10.1088/1361-6528/abc850
[24] Q. He, G. Chen, Y. Wang, X. Liu, D. Xu, X. Xu, Y. Liu, J. Bao, X. Wang. Small, **17**, 2101403 (2021). DOI: 10.1002/smll.202101403
[25] M.M. Shehata, T.G. Abdel-Malik, K. Abdelhady. J. Alloys Comp., **736**, 225 (2018). DOI: 10.1016/j.jallcom.2017.11.097

Translated by D.Kondaurov